

# A survey for high-redshift radio-loud quasars: optical spectroscopy of $S > 0.2$ Jy, flat-spectrum radio sources

I. M. Hook<sup>1</sup>, R. G. McMahon<sup>2</sup>, M. J. Irwin<sup>3</sup> and C. Hazard<sup>2,4</sup>

<sup>1</sup> *U.C. Berkeley Astronomy Dept., Berkeley CA94720, USA, e-mail imh@bigz.berkeley.edu*

<sup>2</sup> *Institute of Astronomy, Madingley Road, Cambridge CB3 0HA, UK*

<sup>3</sup> *Royal Greenwich Observatory, Madingley Road, Cambridge, CB3 0EZ, UK*

<sup>4</sup> *University of Pittsburgh, Pittsburgh, PA 15260, USA*

23 March 2021

## ABSTRACT

We present optical spectroscopic data for a complete sample of 161  $S_{5\text{GHz}} \geq 0.2\text{Jy}$ , flat-spectrum radio sources. The sources were observed as part of a survey for high redshift, radio-loud quasars, and were selected for spectroscopic follow-up based on criteria of red optical colour and unresolved optical counterpart, as measured from APM scans of POSS-I plates. 13 objects from the spectroscopic sample were found to be radio-loud quasars with  $z > 3$ , of which two were previously known. We give positions, E (red) magnitudes, O – E colours, 5GHz radio fluxes, radio spectral indices, optical spectra and redshifts where possible for the spectroscopic sample. We also give finding charts for the  $z > 3$  QSOs. The highest redshift object found is a QSO with  $z = 4.30$  (GB1508+5714, the subject of an earlier Letter). The sample also contains a  $z = 3.05$  QSO, GB1759+7539, which is optically very luminous ( $E=16.1$ ). In addition, spectra are given for 18  $S_{5\text{GHz}} \geq 0.2\text{Jy}$ , flat-spectrum radio sources that do not form part of the complete sample.

**Key words:** surveys – quasars:general – radio continuum:galaxies

## 1 INTRODUCTION

The first quasar to be identified as such was the strong radio source 3C 273, with a redshift of 0.158 (Hazard, Mackey & Shimmins 1963, Schmidt 1963). Since then, radio-selected samples have played an important part in the discovery of quasars and in the study of their evolution.  $V/V_{\text{max}}$  analysis of a complete sample of radio-selected quasars first led to the conclusion that the quasar population is evolving rapidly (Schmidt 1968). Using quasars from the 3CR catalogue, Schmidt found that at constant luminosity, the space density at  $z = 1$  is about 150 and 80 times the local density, for  $q_0 = 0$  and 1 respectively.

Over the past years, much observational effort has gone into the construction of complete samples of quasars in order to determine the luminosity function and its evolution with redshift. The status of the major quasar surveys and selection techniques have been reviewed by Hartwick & Schade (1990) and in two conference proceedings (Osmer et al. 1988; Crampton 1991). At present the quasar population is believed to undergo strong luminosity evolution up to redshifts of  $\sim 2$ , and this evolution slows down between redshifts 2 and 3. Prior to the work described in this paper, the only large complete samples of QSOs with redshifts greater than 3 have been produced from optical surveys (Warren, Hewett & Osmer 1991; Irwin, McMahon & Hazard 1991; Schnei-

der, Schmidt & Gunn 1994). The form of the evolution at these redshifts is less clear-cut than at lower redshifts, and it appears that a combination of luminosity evolution and density evolution is taking place. The space density of the less optically luminous quasars ( $M_B \sim -26$ ) appears to decline rapidly at  $z > 3$  (Schmidt, Schneider & Gunn 1991, Warren, Hewett & Osmer 1994), whereas no evidence for a decline was found for the higher luminosity optically selected quasars ( $M_B < -28$ ) (Hazard, McMahon & Sargent 1986; Miller, Mitchell & Boyle 1990; Irwin et al. 1991).

Evidence for a decline in space density at high redshifts suggests that the epoch of galaxy formation may have been found (with the caveat that quasars probably represent the extreme of the matter distribution and are not necessarily tracers of the galaxy population). There is, however, much controversy over these results owing to the complex, redshift-dependent selection effects which affect optical surveys for high-redshift quasars.

Radio selection methods are less prone to redshift-dependent bias, and the resulting quasar samples can be used to derive the luminosity function independently of optical surveys. Radio fluxes are unaffected by any obscuration arising from dust in foreground galaxies. Also, the spectral energy distribution of quasars at radio wavelengths is smooth and is not complicated by either emission lines

or redshift-dependent intervening absorption so that the effects of  $k$ -corrections are easier to model. Moreover, since the mean radio spectral index of core-dominated, flat-spectrum radio sources is about 0.0, a higher fraction will lie at high redshift compared with samples selected at optical or X-ray wavelengths where spectral indices are typically in the range  $-0.5$  to  $-1.0$ .

In order to find sufficient quasars for a statistical analysis of their space density, it is necessary to survey a large area or go to a faint flux limit. Previous work using radio samples has concentrated on the optical identification of optically faint radio galaxies from bright, large-area radio surveys, e.g. 3C and 4C, or weak radio sources from deep surveys over small areas. These samples were usually selected at low frequency (e.g. 178MHz), which biases their content to a high fraction of steep-spectrum sources, usually identified with galaxies. Surveys at higher frequency contain a higher fraction of flat-spectrum, core-dominated sources, usually identified with quasars.

Optical identification of sources from large-area radio surveys has become more feasible since the advent of measuring machines for determining accurate optical positions and magnitudes from photographic plates. In order unambiguously to identify high-redshift quasars, which have similar colours to those of the stellar sequence, accurate radio positions are needed. The use of the Very Large Array (VLA) to measure positions of sources detected using other instruments has made available large samples with positions accurate to better than 1 arcsec. The use of Schmidt telescopes and radio selection techniques in quasar surveys is described by Hazard (1986).

Recent work in the identification of complete samples of radio sources and their use in luminosity function calculations includes that of Peacock (1985) and Dunlop & Peacock (1990), in which redshifts have been obtained for four radio samples selected at 2.7GHz. The faintest of these samples reaches a flux limit of 0.1Jy and the combined samples contain a total of nearly 200 radio-loud quasars. However, owing to the selection frequency and the small area covered at low flux limits, these samples contain very few high-redshift quasars. Only two quasars have spectroscopically confirmed redshifts above  $z = 3$  in the combined flat- and steep-spectrum samples of Dunlop & Peacock (1990). New data at high redshifts are therefore needed to derive the luminosity function of radio-loud quasars with  $z > 3$ .

We have developed a technique to find radio-loud quasars with  $z > 3$ . The technique involves optical identification of a large number of radio sources, followed by selection of the optically red, unresolved objects. The first results were published in a recent Letter (Hook et al. 1995). The current paper is concerned with the results of spectroscopy of a complete  $S_{5\text{GHz}} \geq 0.2\text{Jy}$  flat-spectrum sample which is briefly described in the following section. The radio data and optical identification procedure will be described in detail in a future paper. The optical identification of the radio sample and selection of the spectroscopic sample are described in Section 3 of this paper. The observations and data reduction are described in Sections 4 and 5 respectively, and the results are presented in Section 6. Finally, tables of redshifts, optical and radio data for the spectroscopic sample and the extra objects observed are given, along with the spectra.

## 2 THE RADIO DATA

Patnaik et al. (1992a) have analysed 5-GHz radio maps from the  $S \geq 25\text{mJy}$  Green Bank (GB) survey (Condon, Broderick & Seielstad 1989) in order to produce a sample of flat-spectrum sources brighter than 0.2Jy. Spectral indices were calculated from the 5-GHz flux densities and the 1.4GHz flux densities from Condon & Broderick (1985,1986).

About 800 flat-spectrum ( $\alpha_{1.4}^5 \geq -0.5$ ,  $S \propto \nu^\alpha$ , where  $\alpha_{1.4}^5$  is the spectral index between 1.4 and 5-GHz) sources in the declination range  $35^\circ \leq \delta(\text{B1950}) \leq 75^\circ$  and with  $|b| \geq 2^\circ.5$  were observed with the VLA (Patnaik, et al. 1992a) giving positions with rms accuracy of  $\sim 12$  milliarcsec. A further  $\sim 800$  flat-spectrum sources in the ranges  $20^\circ \leq \delta(\text{B1950}) \leq 35^\circ$  and  $75^\circ \leq \delta(\text{B1950}) \leq 90^\circ$  were also observed. Those sources with  $\delta > 75^\circ$  originated from the S5 survey (Kühr et al. 1981) and spectral indices for these sources were taken from Kühr et al. (1981). The radio sample therefore contains  $\sim 1600$  sources observed with the VLA, and covers an area of 4.1sr (14000 deg<sup>2</sup>).

Although the 5-GHz flux densities determined by Patnaik et al. were used to define the original radio sample, they have been found to be systematically higher by 10-15 per cent than the flux densities determined by Gregory & Condon (1991) from the same maps. Gregory & Condon have published a comprehensive description of the methods used to determine their flux densities, including a comparison with the Becker, White & Edwards (1991) flux determinations from the same maps. The flux densities were also compared with more accurate measurements at 5-GHz (Kulkarni, Mantovani & Pauliny-Toth 1990) of steep-spectrum sources (i.e. predominantly lobe-dominated and non-varying) from the 408-MHz B3 survey. In this paper we have used 5-GHz flux densities from Gregory & Condon (1991) and 1.4-GHz flux densities from White & Becker (1992) (e.g. Table 1). For sources with  $\delta > 75^\circ$  we have used 5-GHz flux densities from the S5 catalogue (Kühr et al. 1981), and, for sources with  $\delta > 82^\circ$ , above the declination limit of the 1.4-GHz survey, spectral indices between 2.7 and 5-GHz from Kühr et al. (1981) were used. A full comparison of the flux densities will be made in a future paper. We have calculated the effective flux limit of the Patnaik et al. sample to be  $\sim 175\text{mJy}$ . Since Patnaik et al. used high values for the 5-GHz flux, the spectral indices of the sources,  $\alpha_{1.4}^5$ , were estimated to be slightly too flat (i.e.  $\alpha$  more positive if  $S \propto \nu^\alpha$ ) by  $\sim 0.1$ . The effective spectral index limit of the sample is therefore about  $-0.6$ . Occasional steeper (more negative) values of  $\alpha$  will be seen in Tables 1, 3 and 4 since we have used different 1.4-GHz flux densities from those used by Patnaik et al. (1992a) to define the radio sample.

This sample has an advantage over other radio samples for determining the quasar luminosity function in that the contribution from strong lensing will be known explicitly, since all the objects have been observed at high resolution (0.24 arcsec FWHM) using the VLA. Follow up observations to confirm the lenses are underway. At present the known lenses contained in the radio sample are 1422+2309 ( $z = 3.62$ , Patnaik et al. 1992b), 1938+666 (Patnaik & Narasimha 1993) and 0218+357 (Patnaik et al. 1993).

### 3 OPTICAL IDENTIFICATION AND SELECTION OF THE SPECTROSCOPIC SAMPLE

Optical identification of the radio sources was carried out using the Automated Plate Measurement (APM) Facility at Cambridge, U.K. The process involves the digitisation and internal calibration (Bunclark & Irwin 1983) of Palomar Sky Survey (POSS-I) photographic plates in two passbands, E (red) and O (blue). Plates were scanned with  $\sim 0.5$ -arcsec pixels, and the coordinate systems of the two plates covering each field were matched. E and O magnitudes were measured for each detected object, and the images were classified as galaxies, ‘stars’ (i.e. unresolved images) or noise. Various combinations of image parameters are used for this, e.g. moments, ellipticity, etc. The spread in the distribution of each parameter with respect to the stellar locus is found and is used to weight that parameter when they are combined to form a final classification parameter. The mean and spread of the distribution of the combined parameter are found as a function of magnitude, and a statistical correction calculated to convert these to Gaussian distributions with zero mean, rms=1. This is done only for the ‘stellar’ objects. In a second pass the correction is applied to all the images and then the number of standard deviations from a stellar profile,  $N\sigma_c$ , is recorded. For images about 2 magnitudes above the plate limit, the classification is about 90 per cent accurate.

Optical identifications of the radio sources were made on the basis of positional coincidence alone. The rms difference between optical and radio positions,  $\sigma_r$ , was determined by fitting a Rayleigh distribution function to the distribution of  $\Delta r$ , and was found to be 0.7 arcsec. The criterion for positional coincidence was chosen to be  $\Delta r \leq 3.0$  arcsec, i.e.  $\sim 4.3\sigma_r$ . At larger separations the number of background red, stellar sources begins to dominate the number of real red, stellar identifications. Assuming Gaussian statistics, this results in a negligible fraction ( $< 0.01$  per cent) of correct identifications being lost from the sample. In practice the fraction is probably somewhat higher than this owing to non-Gaussian errors which cause the distribution of  $\Delta r$ -values for true identifications to have a longer tail. The background source density of red, stellar objects was estimated from the annulus 10 to 15 arcsec around each source and was found to be  $0.002 \text{ arcsec}^{-2}$ . This gives a false identification rate in a 3.0-arcsec radius of 0.057.

The zero-point for photometry in each field was calculated by assuming that the E plate has a limiting magnitude of 20.0 and by assuming a universal, magnitude-independent position in the colour-magnitude plane for the stellar locus, as described by McMahan (1991). The zero-point of the magnitude system has an rms uncertainty of 0.25mag. A description of the plate material and the steps in the plate measurement and candidate selection, along with a full list of the optical identifications, magnitudes and image classification, will be given in a future paper.

The sample of candidate high-redshift quasars was selected using the APM image classification, O–E colour and positional coincidence of the radio source with an optical counterpart. The basis for the colour selection method is that the O – E colours of QSOs with  $z > 2$  become redder rapidly with redshift, owing to absorption by intervening

Ly $\alpha$  (see fig. 1 in Hook et al. 1995). To define a sample with a high level of completeness at  $z > 3$  we chose a limit of  $O - E \geq 1$ .

$N\sigma_c \leq 3.0$  was chosen as the classification criterion based on the distribution of  $N\sigma_c$  for blue ( $O - E < 1.0$ ) objects within 3.0 arcsec of each radio source, most of which will be QSOs (with  $z < 3$ ). 92 per cent of these blue identifications have  $N\sigma \leq 3.0$ . A limit of  $E \geq 11.0$ mag was also imposed on the spectroscopic sample since  $z > 3$  QSOs are not expected to be brighter than this.

In summary, the selection criteria were (i) positional coincidence,  $\Delta r \leq 3$  arcsec, (ii) red optical colour  $O - E \geq 1.0$ , (iii) unresolved image on the E plate,  $N\sigma_c \leq 3.0$ , (iv)  $E \geq 11.0$  mag. In addition, the optical counterpart had to be bright enough to appear on the E plate, i.e.  $E \leq 20.0$ . The counterpart was not required to be detected on the O plate.

Of the initial radio sample,  $\sim 940$  sources lie in the region covered by the APM scans (i.e. avoiding the galactic plane,  $|b| \geq 20 - 30^\circ$ ), an area of 2.2sr ( $7300\text{deg}^2$ ). 738 of these have optical identifications within 3 arcsec. Of these, 161 satisfy the criteria above. This sample of 161 objects will be referred to as the ‘complete sample’.

Fig. 1 shows the distribution on the sky of the parent radio sample and the complete spectroscopic sample, and a colour-magnitude diagram showing the complete sample is given in Fig. 2. Prior to the start of this project in 1992, 38 of the complete sample had published redshifts, including two with  $z > 3$ . These two are 0636+6801 with  $z = 3.18$  (an S4 source: Kühr 1977, 1980) and 0642+4454 with  $z = 3.41$  (OH471: Gearhart et al. 1972, Carswell & Strittmatter 1973). This left 123 objects requiring spectroscopy. The previously known objects were not re-observed (except one, GB0916+8625). Their properties are summarized in Table 1. There are no known radio-loud,  $z > 3$  quasars within the parent radio sample that do not fulfil the colour criterion  $O - E > 1.0$ .

### 4 OPTICAL SPECTROSCOPY

The aim of the spectroscopic phase of this project was to obtain classification (high-redshift QSO or not) for the complete spectroscopic sample defined above. This does not require redshifts to be obtained for all the objects: for example, many ‘featureless’ spectra could be rejected as possible  $z > 3$  quasars by the lack of Ly $\alpha$  forest absorption. The strategy was therefore to take short exposures at low dispersion to obtain spectra of sufficient quality for the nature of the object and, where possible, the redshift to be determined. In a few cases, where the objects turned out to be particularly interesting, longer exposures were taken (GB1508+5714 and GB1745+6227). In poor weather, spectra were taken of optically brighter identifications which do not necessarily satisfy all the selection criteria described in the previous section. Some of these are slightly resolved on the basis of the APM structure parameter,  $N\sigma_c$ , and some are bluer than the limit  $O - E = 1$ .

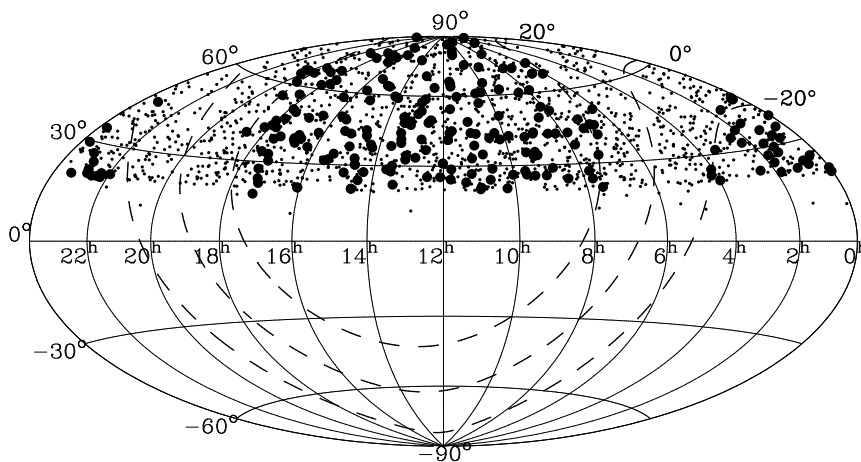


**Figure 1.** Aitoff projection showing the sky distribution of the parent radio sample (points) and identifications satisfying the selection criteria, i.e. the complete spectroscopic sample (filled circles). Dashed lines show the galactic equator and galactic lines of latitude  $|b| = 20^\circ$ .

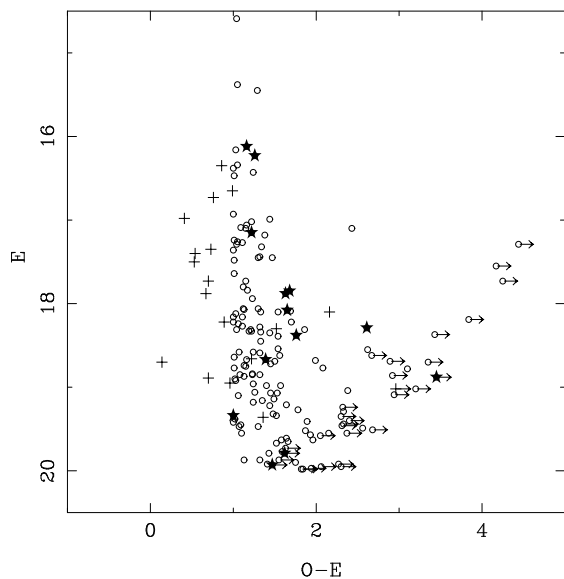


**Figure 2.** Colour-magnitude diagram for the optical identifications of the 0.2Jy sample. The open circles represent objects satisfying the selection criteria for the spectroscopic sample. Crosses show additional objects for which we have obtained spectra. Arrows show limits on O–E colour for objects that were not detected on the O plate. The  $z > 3$  QSOs are shown by star symbols.

#### 4.1 Observational set-up

Most of the spectroscopy was carried out in 1992 October and 1993 April on the 4.2-m William Herschel telescope (WHT), La Palma. The observations were taken using the Durham-RGO Faint Object Spectrograph (FOS-II) or the ISIS double spectrograph. Typical exposure times were 300–600s.

##### 4.1.1 Faint Object Spectrograph

FOS is a fixed-format, low dispersion spectrograph of high throughput, specifically designed for observing faint objects. FOS-II is used at the  $f/11$  Cassegrain focus of the WHT.

A  $385 \times 578$  GEC CCD, coated to improve UV response, was used as a detector. Dispersion is provided by a transmission grating and a cross-dispersing prism which together give a two-order format covering the wavelength range 4000 to  $10500\text{\AA}$ . For this project useful data were obtained only in first order ( $8.7\text{\AA}/\text{pixel}^{-1}$  on the WHT) over the wavelength range  $4800\text{--}9500\text{\AA}$ . FOS-II is described in more detail by Allington-Smith et al. (1989).

##### 4.1.2 ISIS double spectrograph

ISIS is a double spectrograph with arms optimized for blue and red light which was used at the  $f/11$  Cassegrain focus of the WHT. A range of intermediate dispersions are possible from  $120$  to  $8\text{\AA}/\text{mm}^{-1}$ . For this project the lowest dispersion was required, and a grating with  $158$  lines/mm and a dichroic at  $\sim 5400\text{\AA}$  were used. The gratings were arranged so that the blue part of the spectrum was centred on  $4600\text{\AA}$  and covered a range of  $2950\text{\AA}$  while the red was centred on  $7000\text{\AA}$  and covered a range of  $3380\text{\AA}$ .

On the red arm an EEV  $1242 \times 1152$  CCD with  $22.5\mu\text{m}$  pixels was used as detector. On the blue arm a thinned Tektronix CCD with  $1024 \times 1024$  ( $24\mu\text{m}$ ) pixels was used.

#### 4.2 Observations

A total of six nights were allocated to this project in 1992 October and 1993 April. Prior to that, some observations were carried out interspersed with other programmes. Table 2 shows the instrument used during each run, and the number of objects observed from the complete sample. The observations on June 28/29 and August 17–19 were carried out in the context of the PATT service observation programme.

For all observations, the width of the slit was adjusted to be compatible with the seeing at the time of observation ( $1\text{--}2$  arcsec). All observations were taken with the slit at the parallactic angle. Almost all the objects were too faint to be easily visible on the acquisition TV, so accurate offsetting from nearby stars was used to position the target object

**Table 1.** Objects in the complete sample that had published redshifts prior to the start of the project in 1992. These objects were taken from Hewitt & Burbidge (1987, 1989, ‘HB’) and from Véron-Cetty & Véron (1991, ‘V91’). Redshifts and object classifications are from NED† (references given there) except where stated.

Optical Position			$z$	$N\sigma_c$	E	O–E	$\Delta r$	$S_5$	$\alpha_{1.4}^5$	Comments	
$\alpha$	1950		$\delta$		mag	mag	"	mJy			
01 09	23.58	22 28	44.3	–	0.12	14.59	1.04	0.55	260	–0.11	BL Lac
01 49	31.70	21 52	19.9	1.32	0.55	18.06	1.12	0.99	1060	–0.21	QSO
02 01	56.24	36 34	57.0	2.91	0.68	17.45	1.30	1.06	349	–0.41	QSO
04 09	44.67	22 57	27.5	1.21	0.44	18.10	1.54	0.03	1000	–0.20	QSO
04 54	57.15	84 27	52.7	0.11	0.77	17.10	1.15	0.38	1398	0.38*	QSO
06 36	47.38	68 01	25.9	3.18	1.95	16.23	1.26	1.83	499	1.06	QSO
06 42	53.03	44 54	30.5	3.41	0.67	17.88	1.63	0.37	1191	0.55	QSO; $z$ is from V91, $z = 3.396$ in NED
07 10	3.31	43 54	26.3	0.52	0.72	19.73	> 1.63	0.27	1629	–0.09	QSO
07 16	4.43	33 12	42.7	–	1.24	18.06	1.30	1.07	364	0.44	listed in V91, no optical ID in NED
07 16	12.83	71 26	15.0	–	0.05	14.42	1.03	0.88	788	–0.02	BL Lac
07 45	35.75	24 07	55.3	0.41	1.97	18.31	1.04	0.45	1196	0.15	QSO
08 14	51.64	42 32	7.0	0.26	0.28	18.85	1.08	0.90	1891	0.20	BL Lac
08 27	54.37	24 21	7.1	2.05	1.33	16.16	1.03	0.75	672	–0.03	QSO; HB give $z = 0.94$
08 28	47.96	49 23	32.2	0.55	1.11	18.34	1.33	0.90	363	–0.80	BL Lac
08 49	4.49	28 45	18.3	1.27	0.53	19.34	1.52	0.92	422	0.19	QSO
09 16	11.95	86 25	16.9		0.56	18.07	1.13	1.23	253	0.21*	BL Lac; also observed in this work
09 17	40.24	62 28	37.9	1.45	1.01	18.16	1.11	1.00	1322	0.06	QSO
09 54	57.72	65 48	15.1	0.37	0.19	15.45	1.29	0.94	1417	0.61	BL Lac
10 30	7.85	41 31	34.1	1.12	0.64	17.36	1.00	0.70	485	–0.37	QSO
10 48	10.41	34 46	5.6	2.52	1.43	18.98	1.40	0.36	298	–0.46	QSO
10 53	35.84	81 30	36.3	0.71	0.09	18.09	1.69	1.08	770	0.64	Galaxy
11 38	40.07	65 52	59.9	0.81	1.28	17.73	> 4.25	0.84	184	–0.69	Galaxy
12 31	50.22	48 10	22.6	0.38	0.91	16.47	1.01	0.31	278	–0.23	Listed in V91, no ID in NED
12 54	4.89	57 08	37.3	0.04	1.84	11.08	1.15	1.46	419	0.29	Galaxy
13 08	7.54	32 36	39.4	1.00	2.92	18.59	1.32	1.06	1131	–0.28	BL Lac
14 13	22.73	37 20	15.5	2.36	0.08	17.29	1.04	0.77	383	0.04	QSO
14 17	43.05	38 35	30.6	1.82	0.04	19.40	> 2.40	1.83	871	0.16	QSO
14 24	44.17	24 01	25.0	–	0.33	15.38	1.05	1.16	316	–0.24	BL Lac
14 42	52.98	63 45	3.8	1.38	0.33	17.27	1.11	0.58	456	–0.32	Galaxy
15 20	56.25	34 24	46.4	1.31	0.79	18.22	1.00	0.70	147	–0.34	QSO
16 38	48.12	39 52	30.3	1.66	0.39	17.24	1.01	0.70	1285	0.53	QSO
17 22	23.36	33 05	42.9	1.87	0.31	18.85	1.32	0.75	435	0.23	QSO
17 32	40.46	38 59	46.0	0.97	0.01	18.87	1.13	1.09	561	–0.26	BL Lac
17 38	12.61	49 56	35.5	1.55	0.24	17.48	1.01	0.86	478	–0.13	QSO
18 03	39.27	78 27	54.0	0.68	1.61	13.93	1.50	0.31	2633	0.27	BL Lac
18 23	14.94	56 49	18.0	0.66	1.19	17.02	1.22	0.22	1135	–0.21	QSO
22 17	15.98	21 26	6.4	1.52	0.48	18.62	> 2.67	1.20	248	–0.12	QSO
22 51	44.32	24 29	23.6	2.33	0.27	17.26	1.05	1.30	937	–0.62	QSO

**Notes:**

**Optical data:** APM measurements of optical positions, E magnitudes, O–E colours and the classification parameter  $N\sigma_c$  are described in McMahon et al. (in preparation).

**Radio data:** 5GHz fluxes  $S_5$  from Gregory & Condon (1991) are given for sources with  $\delta < 75^\circ$ . For higher declination sources, 5GHz fluxes are taken from the S5 catalog (Kühr et al. 1981). For  $\delta < 82^\circ$ , the spectral indices  $\alpha_{1.4}^5$  ( $S \propto \nu^\alpha$ ) were calculated using these 5GHz fluxes and 1.4GHz fluxes from White & Becker (1992). Limits are given for objects below the flux limit of the 1.4GHz catalog, 100mJy. For  $\delta > 82^\circ$ , above the declination limit of the 1.4GHz catalog, we give the 2.7GHz to 5GHz spectral indices from Kühr et al. (1981), and mark these objects with a ‘\*’ in the  $\alpha_{1.4}^5$  column.

† The NASA/IPAC Extragalactic Database (NED) is operated by the Jet Propulsion Laboratory, California Institute of Technology, under contract with the National Aeronautics and Space Administration.

in the slit. Spectrophotometric standards were observed to calibrate the spectra.

All ISIS observations were made with a long slit ( $\sim 2$  arcmin). The FOS-II observations were made with a short slit (projected length  $\sim 20$  arcsec) to prevent the first- and second-order spectra overlapping. The CCD chips were win-dowed in the spatial direction to reduce the readout time.

Further observations of GB1508+5714 were carried out on 1993 April 17. Three 900s observations were obtained

with the red arm and two 1500s observations with the blue arm, with a 1.5 arcsec spectrographic slit. Red and blue observations of the flux standard HD 84937 were used to flux-calibrate the data.

GB1745+6227 was re-observed on 1992 August 1 (a service night). Seven 900-s observations were obtained with the red arm, and six 900-s observations with the blue arm. Red and blue observations of the flux standard BD +40° 4032 were used to obtain relative flux calibration.

**Table 2.** Dates of observations, instruments used and number of objects observed from the complete sample.

UT date	Instrument	No. Observed
20 – 25, 27 Apr 1992	FOS-II/ISIS	22
02 – 04 Oct 1992	FOS-II/ISIS	21
09 – 12, 17 Apr 1993	FOS-II/ISIS	75
28 Jun 1993	ISIS	1
17 – 18 Aug 1993	ISIS	1
9 – 10 Jun 1994	FOS-II	2

## 5 DATA REDUCTION

The reduction of data was carried out using standard software from the IRAF package. The steps taken in the data reduction are summarized below.

(1) *Overscan correction, bias correction and flat-fielding.* A linear ramp was fitted to the overscan region in the direction perpendicular to the dispersion axis, and was subtracted from the 2D frames. For each observing run, a combined bias frame was subtracted from the 2D frames.

Flat-field frames were taken on each run using a tungsten lamp to illuminate the slit, and were used to correct for pixel-to-pixel sensitivity variations.

(2) *Extraction of spectra.* The object spectra were located and traced along the chip. Typically the ISIS spectra curved by less than a pixel from one end of the chip to the other, whereas the FOS-II spectra shift by about 35 pixels, as a result of the cross-dispersing prism. The functional form of the tracing function was specified to be a Legendre polynomial of order 4 for FOS-II and order 3 for ISIS. The sky level was determined by interpolating between specified regions on either side of the spectrum, and was subtracted. The extraction was variance-weighted using the variances determined from the data and CCD characteristics.

(3) *Wavelength calibration and flux calibration.* Cu-Ar+Cu-Ne arc lamp spectra were used to wavelength calibrate the data. Non-blended emission lines were identified, and a pixel-to-wavelength calibration curve was found by fitting a third-order polynomial to the calibration points. Typical rms residuals from the fit were 0.3Å for FOS-II and 0.2Å for ISIS. A few spectra were calibrated using emission and absorption features in the sky spectra. Typical rms residuals derived using sky spectra were 0.3Å for ISIS, and 0.8-1Å for FOS-II.

Observations of spectrophotometric standards were used to flux-calibrate the data. Usually only relative flux calibration over the wavelength range of each spectrum was required. Some observations were carried out through thin and patchy cloud which causes wavelength-independent extinction. The relative flux calibration is unaffected, however, and the resulting spectra can still be used for spectral index determination.

The flux calibration procedure was checked by flux-calibrating the standards and overlaying the calibration points. It was found that calibration was reliable over the wavelength ranges 5500-8600Å (ISIS red), 3600-5500Å (ISIS blue) and 4950-9500Å (FOS-II).

The high-quality ISIS spectra that were taken of the

highest redshift objects were corrected for atmospheric absorption using observations of featureless B stars.

## 5.1 Measurement of redshifts

Redshifts were estimated for objects that had obvious emission lines. For quasars with redshifts above  $\sim 2.2$  redshifts could be measured using the broad emission lines CIV (rest wavelength 1549Å) and CIII] (1909Å). Ly $\alpha$  (1216Å) was also used to identify these objects (depending on the wavelength coverage of the spectrum) but the redshift based on that line is an upper limit since the peak of Ly $\alpha$  is shifted towards the red due to absorption by the Ly $\alpha$  forest. In some objects the NV (1240Å) and SiIV/OIV] (1400Å) features could also be used to derive the redshift. For objects with redshifts less than  $\sim 0.8$ , the [OIII](5007/4959Å) and H $\beta$ (4861Å) emission lines could be identified. Intermediate redshift objects could be identified by the MgII (2798Å) and CIII] emission lines.

The observed wavelengths were measured from the centroids of the lines (calculated in IRAF) unless the line profile was visibly affected by sky absorption. When more than one clean line was visible, an average redshift was taken, otherwise the redshift was based on the cleanest (usually strongest) line.

## 6 RESULTS AND DISCUSSION

After the 1993 August observing run the spectroscopic observations of the complete sample defined in Section 1 were essentially complete to the limit of the POSS-I plates,  $E \sim 20$ . The spectra of objects that satisfy all the selection criteria are shown in Fig. 6, and their properties are tabulated in Table 3. Spectra of the extra objects are shown in Fig. 4, and their properties given in Table 4. Some of the ISIS spectra of lower signal-to-noise ratio have been smoothed (using a Gaussian smoothing function with  $\sigma = 2$  pixels). Three objects in the complete sample still have inconclusive spectra. In two cases the objects were not detected (possibly because the POSS-I identifications were chance coincidences with stars that have since moved), and in the third case the signal-to-noise ratio was too low. One other object remains to be observed. The objects with poor or no spectra are listed in Table 5. Therefore, of the 123 objects requiring spectroscopy, we now present spectra for 119, plus one previously known object that was re-observed (GB0916+8625).

In the complete sample a total of 11 new quasars with  $z > 3$  were found, of which four have  $z > 3.5$ . Since 120 objects were observed, the efficiency of the survey for  $z > 3$  QSOs is approximately 1 in 10. The  $z > 3$  QSOs are marked on the colour-magnitude diagram (Fig. 2) with star symbols. A further 12 new quasars in the range  $2 < z < 3$  were found (but note that the colour selection criterion means that the sample is substantially incomplete for  $z < 3$ ). The highest redshift object found was a quasar with a redshift of  $z = 4.30$ , the first known radio-selected quasar with  $z > 4$ . This object has been the subject of an earlier paper (Hook et al. 1995).

The remaining objects were found to be low-redshift ( $z < 2$ ) quasars, emission-line galaxies and objects with featureless spectra which could be ruled out as possible high-

**Figure 3.** Objects satisfying the selection criteria of the complete sample.

**Figure 4.** Objects which did not satisfy all the selection criteria. The properties of these objects are summarised in Table 4.

redshift quasars. Redshift estimates are now available for 90 objects in the complete sample (including previously known objects), and their redshift distribution is shown in Fig. 5.

Assuming the background source density of red, stellar objects to be  $0.002 \text{ arcsec}^{-2}$ , we expect a false identification rate in a 3.0 arcsec radius of 0.057 (see Section 3), or nine objects in the sample of 161. This compares to the two objects that were not detected and could be chance coincidences with stars that have since moved. It is also possible that some of the objects that we found to have ‘featureless’ spectra are chance coincidences with foreground stars.

The  $z > 3$  QSOs will be combined with previously existing data to calculate the luminosity function, the subject of a future paper.

### 6.1 The new sample of $z > 3$ QSOs

A summary of the 13  $z > 3$  QSOs in the complete sample is given in Table 6. Histograms showing the distributions of spectral index, colour, E magnitude and classification parameter  $N\sigma_c$  for all the quasars with  $z > 3$  included in the new sample are shown in Fig. 6. The distributions of colour, E magnitude, spectral index and 5-GHz flux  $S_5$  with redshift are shown in Fig. 7. As can be seen from these, all the  $z > 3$  quasars lie well within the criterion for having a stellar (unresolved) optical image ( $N\sigma_c \leq 3.0$ ). In addition, most of the quasars with  $z > 3$  have O–E colours significantly greater than the imposed limit of 1.0. This suggests that any incompleteness introduced by the colour cut and classification criterion is small. The distribution of spectral indices appears to have a mean of about zero, and no obvious trend with redshift is seen. Incompleteness introduced by other factors, such as the optical limit for identifications, will be discussed in a future paper, although it is interesting to note that the distribution of E magnitudes is fairly flat, and does not ‘pile up’ at the limit of  $E = 20$ .

Five of the quasars in Table 6 are radio sources included in the CJ1 (Polatidis et al. 1995) or CJ2 survey (Taylor et al. 1994). These are GB0636+6801, GB0642+4454, GB0749+4239, GB1526+6701 and GB1745+6227.

Two  $z > 3$  quasars are known to lie within the survey area but were not found by this survey. A gravitational lens, 1422+2309, with a redshift of 3.62 has been discovered as part of the new VLA/MERLIN search for small-separation lenses (Patnaik et al. 1992b). This source is included in the 0.2Jy sample and satisfies all the selection criteria used to define the complete sample of  $z > 3$  quasars except that its optical image is classified as ‘merged’ by the APM software, and it did not meet the  $N\sigma_c \leq 3.0$  criterion. It was therefore not included in the spectroscopic sample. Also a  $z = 3.1$  quasar, GB1839+389, was found as the result of spectroscopic observations of CJ2 sources (Henstock et al., in preparation). This object is also included in the 0.2Jy sample but the optical image was classified as highly non-stellar on the E plate.

**Table 6.**  $z > 3$  objects in the complete sample. See Table 1 for an explanation of the column headings.

Name	$z$	E mag	O–E mag	$S_5$ mJy	$\alpha_{1.4}^5$
GB0148+2502	3.10	19.79	> 1.62	237	0.28
GB0229+2304	3.42	19.93	> 1.47	457	0.18
GB0636+6801	3.18	16.23	1.26	499	1.06
GB0642+4454	3.41	17.88	1.63	1191	0.55
GB0749+4239	3.59	18.08	1.65	461	−0.33
GB1013+2052	3.11	18.67	1.39	976	0.18
GB1147+4348	3.02	19.34	1.00	187	−0.02
GB1338+3809	3.10	17.85	1.68	305	0.00
GB1508+5714	4.30	18.88	> 3.45	282	0.50
GB1526+6701	3.02	17.15	1.22	417	−0.02
GB1745+6227	3.89	18.29	2.61	580	−0.22
GB1759+7539	3.05	16.12	1.16	145	> 0.29
GB2223+2024	3.56	18.38	1.76	143	−0.31

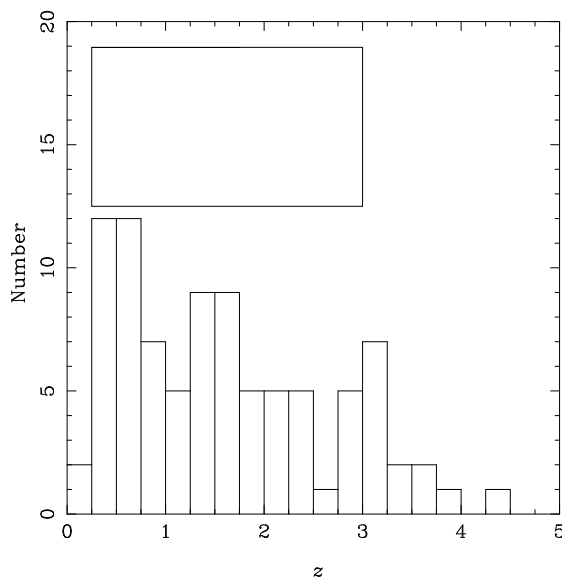


**Figure 5.** Histogram of redshifts obtained for the complete sample. The histogram includes the previously known objects and objects with uncertain redshifts, giving a total of 90 objects. Objects with spectra from which redshifts could not be measured (71 of the complete sample) are represented by the rectangle. It is unlikely that any of these have  $z > 3$  (see text for explanation).

Finding charts for the 13  $z > 3$  quasars in the complete sample are given in Fig. 8.

### 6.2 Notes on individual objects

*GB0003+3803.* Stickel & Kühr (1994) also find  $z = 0.23$ .  
*GB0024+3452.* Stickel & Kühr (1993b) also find  $z = 0.33$ .

**Table 3.** Objects in the complete sample which we have observed with WHT. Spectra for these objects are given in Figure refjbspec. See Table 1 for a description of the column headings. Redshifts are given for objects with obvious emission features. A ‘\*’ indicates an object with an uncertain redshift, e.g. when only one line is visible.

Optical Position			$z$	$N\sigma_c$	E	O–E	$\Delta r$	$S_5$	$\alpha_{1.4}^5$	Date	
$\alpha$	1950		$\delta$		mag	mag	"	mJy		Obs.	
00 03	22.31	38 03	32.4	0.23	1.75	17.10	2.43	0.97	549	−0.07	10/92
00 20	45.98	25 22	40.2		0.97	19.51	> 2.68	2.72	130	> 0.21	10/92
00 24	2.78	34 52	6.6	0.33	2.19	17.45	1.47	0.33	453	−0.47	10/92
01 09	24.75	35 06	24.9	0.45	0.19	17.84	1.17	0.95	362	0.00	10/92
01 19	58.40	29 38	32.9		1.33	17.64	1.01	0.28	154	−0.06	10/92
01 22	9.46	27 49	34.6	0.71	1.87	18.19	> 3.84	0.54	228	0.25	10/92
01 29	46.04	43 10	8.7		0.87	18.67	1.16	0.89	347	0.37	10/92
01 30	48.60	38 07	36.8		0.24	19.02	> 3.20	0.93	204	−0.61	10/92
01 48	18.00	25 02	38.9	3.10	0.75	19.79	> 1.62	0.30	237	0.28	10/92
01 48	37.17	27 29	52.8	1.26	1.11	18.84	1.23	0.95	991	0.28	08/93
02 17	49.86	32 27	23.3	1.62	1.43	17.44	1.32	1.06	618	−0.34	10/92
02 29	29.47	23 04	44.2	3.42	2.53	19.93	> 1.47	0.28	457	0.18	10/92
02 30	18.23	34 29	44.0	0.50	2.47	18.77	2.08	0.97	223	−0.03	10/92
03 25	37.21	31 28	52.1	0.46	1.89	18.98	1.57	0.09	245	0.45	10/92
04 03	24.78	25 03	28.2	0.68*	0.23	19.10	1.06	0.76	212	> 0.59	10/92
06 10	52.79	51 03	7.9	1.59*	1.60	18.64	1.01	1.80	202	0.20	04/93
07 07	2.72	47 37	9.9		0.20	13.00	1.17	2.69	906	−0.06	04/93
07 47	2.64	27 07	59.7	1.54*	1.45	19.58	> 2.05	0.11	139	−0.58	04/93
07 49	21.57	37 38	10.2	0.44	1.17	19.98	> 1.82	1.62	208	−0.04	04/93
07 49	35.26	42 39	17.7	3.59	0.19	18.08	1.65	0.94	461	−0.33	04/93
07 53	10.94	51 59	2.2	1.33*	2.85	18.10	1.33	1.33	196	0.43	04/93
08 05	50.51	53 50	15.2		2.24	19.77	1.59	1.05	197	0.07	04/93
08 30	11.07	60 30	3.3	0.72	1.60	19.22	1.44	1.67	309	0.14	04/93
08 30	31.96	42 34	19.0		0.67	16.99	1.44	0.47	341	−0.38	04/93
08 59	12.84	43 22	4.3	2.41	1.15	19.55	1.10	1.21	324	−0.02	04/93
09 00	58.72	42 50	0.4		0.25	19.90	1.75	0.99	718	−0.52	04/93
09 03	18.88	25 49	36.9	0.48	2.51	19.04	2.38	1.32	272	−0.62	04/92
09 08	43.63	34 01	36.9		1.75	18.62	1.56	1.10	250	−0.67	04/92
09 11	34.07	35 24	31.6	1.07*	2.04	19.47	1.30	1.79	321	0.28	04/93
09 16	11.95	86 25	16.9		0.56	18.07	1.13	1.23	253	0.21*	04/93
09 20	19.83	41 38	20.4		1.07	19.57	1.93	0.92	183	0.12	04/93
09 24	51.80	73 17	12.3		1.93	19.35	> 2.30	0.21	206	0.17	04/93
09 27	52.76	35 16	49.9		0.12	19.18	1.24	1.12	383	−0.08	04/93
09 37	21.97	26 17	7.1		1.03	19.21	1.64	0.76	326	0.04	04/92
09 38	54.56	27 42	19.0		2.39	17.73	1.15	2.80	246	0.07	04/93
09 55	22.28	50 54	19.0	1.15*	0.75	18.74	1.13	0.83	173	−0.23	04/93
10 00	52.32	26 19	45.9		1.56	18.31	1.21	0.20	274	−0.46	04/93
10 09	51.79	40 53	54.8		1.27	19.46	> 2.31	1.84	209	−0.58	04/92
10 13	58.30	61 31	27.2	2.80	0.65	18.12	1.03	0.27	631	0.44	04/93
10 13	59.33	20 52	47.8	3.11	0.76	18.67	1.39	1.45	976	0.18	04/93
10 17	26.37	43 36	0.8	1.96*	1.04	18.27	1.11	1.80	232	0.33	04/93
10 23	13.10	74 43	43.7		0.65	18.72	1.45	0.33	204	0.03	04/93
10 30	32.56	61 06	36.0		1.44	19.32	1.48	1.05	579	−0.22	04/93
10 31	55.92	56 44	18.5	0.46	2.08	19.92	> 2.27	0.37	1200	−0.30	04/93
10 40	25.20	24 24	19.4		1.21	17.09	1.09	0.35	364	0.09	04/93

*GB0035+4120.* Stickel & Kühr (1993b) also find  $z = 1.35$ .

*GB0707+4737.* Stickel & Kühr (1994) give the identification as an 18.2-mag quasar with  $z = 1.292$ . However, the APM scan and the digitized sky survey image show only one bright ( $E \sim 13$ ) object at the radio position. Visual inspection of the POSS-I E and O plates and the POSS-II  $B_J$  plate of the same field reveals that GB0707+4737 is slightly elliptical on the POSS-II plate and there is evidence for a second object in the south-easterly direction on the POSS-I O plate. A contour plot given in Meisenheimer & Röser (1983) shows the fainter identification close to the bright star.

*GB0927+3516.* Henstock (in preparation) also finds this to be featureless after 2000s on the Isaac Newton Telescope.

*GB1030+6106.* A tentative redshift  $z = 0.336$  is given by Stickel & Kühr (1994).

*GB1031+5644.* Aller, Aller & Hughes (1992) report  $z = 0.45$  (compared with our measurement of  $z = 0.46$ ).

*GB1105+4347.* Henstock (in preparation) finds  $z = 1.226$  also.

*GB1124+455.* Henstock (in preparation) also finds  $z = 1.811$ , as do Bade et al. (1995).

*GB1144+5413.* Stickel & Kühr (1994) find  $z = 2.201$  and

Table 3 – continued

$\alpha$	Optical Position			$z$	$N\sigma_c$	E	O–E	$\Delta r$	$S_5$	$\alpha_{1.4}^5$	Date
	1950	$\delta$									
10 56	58.43	21 13	27.9	0.40	0.80	18.35	1.44	0.24	230	0.53	04/93
10 58	26.65	20 36	52.7	1.66*	0.92	19.79	1.43	0.47	159	> 0.36	04/93
10 59	59.91	79 49	3.0		2.48	19.95	> 2.06	0.36	278	-0.40	04/93
11 05	35.16	43 47	9.5	1.22*	1.60	19.52	1.87	0.74	375	0.27	04/93
11 07	46.02	48 34	9.6	0.74	2.60	19.24	> 2.32	0.25	256	-0.51	04/93
11 08	5.59	85 28	15.3	2.85	1.40	19.14	1.49	0.80	108	0.29*	04/93
11 08	48.70	33 09	14.0		0.87	19.45	1.09	0.52	205	-0.03	04/93
11 21	53.23	23 24	24.2		0.59	19.29	2.33	1.06	149	> 0.31	04/92
11 25	23.01	59 41	46.3		0.29	19.95	> 2.30	1.32	393	0.06	04/93
11 38	26.30	64 26	42.3		0.16	19.41	1.89	1.32	334	0.15	04/92
11 40	55.77	66 50	9.4	2.32	0.24	18.33	1.22	1.11	246	0.19	04/93
11 43	0.32	44 37	1.4	0.30	2.52	17.29	> 4.44	0.49	245	-0.46	04/93
11 44	4.47	54 13	22.3	2.19*	1.17	19.63	1.58	1.29	484	0.14	04/93
11 47	39.69	43 48	46.4	3.02	1.71	19.34	1.00	1.00	187	-0.02	04/93
11 51	19.00	40 53	32.7	0.92*	0.52	19.67	1.52	1.55	380	-0.48	04/93
12 00	58.33	31 05	43.4		1.12	19.97	> 1.94	1.32	150	-0.13	04/93
12 26	27.31	49 14	35.6		0.89	18.58	1.24	0.39	326	-0.24	04/93
12 26	48.63	63 51	35.4		2.60	18.70	> 3.35	0.68	308	-0.07	04/92
12 27	44.35	25 34	40.8		1.77	16.34	1.05	0.46	425	-0.34	04/93
12 32	39.28	36 37	49.6	1.60	0.20	19.06	1.26	1.04	250	0.65	04/93
12 42	26.34	41 04	29.7	0.81	0.52	19.07	1.45	0.64	707	-0.65	04/93
12 46	7.27	58 36	49.5		2.33	14.10	1.31	0.29	414	0.43	04/93
12 50	16.34	33 27	15.3		0.28	19.44	> 2.33	0.44	182	-0.10	04/92
12 50	58.19	53 17	27.2		0.97	16.38	1.00	0.85	396	-0.24	04/93
12 57	18.83	51 57	5.9		0.15	19.87	> 1.55	0.06	247	-0.11	04/93
13 00	50.66	69 18	57.3	0.57	2.52	19.61	1.64	1.44	190	0.12	04/93
13 08	41.32	47 09	47.4		1.07	19.07	1.53	0.76	393	0.07	04/93
13 10	32.91	48 44	23.6		1.32	19.98	> 1.84	0.78	224	0.13	04/93
13 20	41.06	39 27	47.5	2.98	0.99	17.06	1.16	0.76	230	0.57	04/93
13 22	21.87	47 58	55.9	2.26	2.07	19.47	1.07	1.03	237	0.18	04/93
13 24	37.12	22 26	22.5	1.40*	1.36	17.18	1.38	0.32	849	1.01	04/93
13 25	10.66	43 41	59.0	2.08	0.96	18.45	1.33	1.28	533	-0.22	04/93
13 30	47.33	27 40	40.7		1.51	18.69	1.50	0.24	161	-0.27	04/93
13 38	11.09	38 09	53.5	3.10	0.08	17.85	1.68	0.60	305	0.00	04/92
13 38	56.79	28 31	12.0	1.31*	0.64	19.55	2.15	1.08	172	> 0.43	04/92
13 57	41.94	76 57	53.3		0.59	18.39	1.54	0.69	844	0.34	04/93
14 00	7.22	58 50	8.0		0.68	18.90	1.02	0.59	220	0.04	04/93
14 17	45.13	27 20	9.4		0.35	18.96	1.24	0.32	414	-0.93	04/93
14 32	9.41	42 16	21.7		0.00	17.80	1.12	0.76	353	0.19	04/93
14 33	3.68	20 34	22.1		0.35	18.28	1.32	0.68	215	-0.43	04/92
14 35	49.41	30 15	3.8		1.87	19.38	1.02	0.45	132	> 0.22	04/93
14 36	36.23	44 31	6.5	2.10	0.96	18.69	> 2.89	0.39	279	0.37	06/93
14 39	54.00	32 47	5.4	2.12	0.76	18.77	1.01	0.69	340	-0.25	04/93
14 51	43.01	27 00	43.6		0.85	18.85	1.23	0.64	354	-0.44	04/93
14 56	46.89	37 32	16.7		0.67	18.22	1.70	0.77	591	0.45	04/92

Xu et al. (1994) find  $z = 2.20$  (compared with our tentative  $z = 2.19$ ).

*GB1145+2652*. Bade et al. (1995) also find  $z = 0.867$ .

*GB1151+4053* Henstock (in preparation) finds  $z = 0.916$ . Our spectrum is consistent with this.

*GB1202+5245* Owen, Ledlow & Keel (1995) also find  $z = 2.73$ .

*GB1206+4136* Henstock (in preparation) also finds this to be featureless after 2500s on the INT.

*GB1218+4428* Henstock (in preparation) also finds  $z = 1.345$ .

*GB1242+4104* Xu et al. (1994) also find  $z = 0.813$ .

*GB1246+5836* This is classified as a featureless BL Lac by Vermeulen & Taylor (1995) and by Fleming et al. (1993).

*GB1250+5317* Henstock (in preparation) also finds this to be featureless after 600s on the INT.

*GB1325+4341* Stickel & Kühr (1994) give  $z = 2.073$  (compared with our  $z = 2.08$ ).

*GB1432+4216* Vermeulen et al. (1996) find  $z = 1.240 \pm 0.004$  for this source.

*GB1456+3732* Vermeulen et al. (1996) obtain  $z = 0.333 \pm 0.001$  for this source, based on weak [OII], [OIII] and H $\alpha$  lines that are not visible in our spectrum.

*GB1508+5714* This is the highest redshift object found in our sample, a quasar with  $z = 4.30$ . This quasar is the first known radio-selected quasar with  $z > 4$ . It has an O–E colour of  $> 3.44$  and an E magnitude of 18.9, and is such a red object that it did not appear on the O plate.

**Table 3** – *continued*

$\alpha$	Optical Position			$z$	$N\sigma_c$	E mag	O–E mag	$\Delta r$ "	$S_5$ mJy	$\alpha_{1.4}^5$	Date Obs.
	$\alpha$	1950	$\delta$								
15 08	45.19	57 14	2.6	4.30	1.45	18.88	> 3.45	0.45	282	0.50	04/92
15 20	4.78	43 47	19.4	2.18	0.19	18.37	> 3.43	1.64	245	0.40	04/93
15 26	12.05	67 01	16.1	3.02	0.89	17.15	1.22	0.72	417	–0.02	04/92
15 32	31.55	48 33	38.3		1.09	17.55	> 4.17	1.15	217	–0.30	04/93
15 33	58.63	31 36	22.8	1.87	2.57	19.65	1.66	0.67	137	–1.26	04/93
15 38	54.02	61 23	31.7		0.65	19.16	1.35	1.77	252	–0.53	04/92
15 45	53.06	49 46	18.2	0.70	1.64	19.63	1.96	1.99	549	–0.42	04/93
16 03	54.09	20 40	9.9		2.15	18.55	2.62	0.43	182	0.24	04/92
16 16	34.54	36 39	14.9		0.87	18.54	1.54	0.42	268	–0.50	04/92
16 23	27.65	57 48	4.4		1.85	17.32	1.34	0.71	590	0.13	04/92
16 29	55.14	49 34	0.2	0.52	1.36	18.31	1.86	0.30	394	0.16	04/93
16 30	17.64	74 37	22.1	0.70	0.49	18.68	1.99	1.49	175	–0.63	04/93
16 30	30.00	77 13	15.4		2.07	18.58	1.07	0.26	174	–0.83	04/93
16 46	50.83	41 09	16.0	0.85	1.48	19.42	1.00	0.92	191	–0.51	04/93
16 51	16.73	39 07	42.8		0.53	19.87	1.32	1.14	308	–0.07	04/93
17 07	56.14	77 59	52.1		1.05	18.16	1.00	0.71	232	–0.10	04/93
17 14	3.75	21 55	29.4		0.75	19.27	1.78	0.80	716	0.07	04/92
17 18	5.57	23 38	28.8	1.86*	0.80	19.09	> 2.94	0.09	150	–0.43	04/93
17 45	47.98	62 27	55.2	3.89	0.03	18.29	2.61	1.06	580	–0.22	04/92
17 47	29.53	43 22	42.4		0.64	16.93	1.00	0.80	367	0.06	04/93
17 50	20.94	50 56	16.6		2.93	18.86	> 2.92	1.17	192	–0.38	04/92
17 59	33.84	75 39	22.4	3.05	0.31	16.12	1.16	0.50	145	> 0.29	04/93
21 57	53.68	21 23	31.3		0.67	18.24	1.06	0.19	251	0.05	10/92
22 14	52.80	20 09	47.5		0.97	16.43	1.24	1.32	221	–0.48	06/94
22 23	13.32	20 24	58.5	3.56	0.93	18.38	1.76	0.86	143	–0.31	06/94
22 46	34.80	20 51	9.5		1.79	18.92	1.03	0.94	771	0.12	10/92
23 07	9.24	26 52	15.5	0.27	2.65	18.78	3.10	1.21	137	–0.54	10/92
23 19	57.66	44 29	13.9		0.35	19.92	1.41	0.95	366	0.14	10/92
23 41	51.56	29 35	41.4		1.19	18.75	1.15	0.45	190	–0.35	10/92
23 42	20.71	34 17	9.3	2.99	1.17	18.33	1.19	0.68	146	0.07	10/92

**Table 4.** Objects observed which do not satisfy the selection criteria of the complete sample.

$\alpha$	Optical Position			$z$	$N\sigma_c$	E mag	O–E mag	$\Delta r$ "	$S_5$ mJy	$\alpha_{1.4}^5$	Date Obs.
	$\alpha$	1950	$\delta$								
00 35	41.55	41 20	37.2	1.35*	3.87	19.36	1.36	0.31	1114	0.73	10/92
08 24	10.19	52 27	54.0	0.34	3.13	18.10	2.16	0.86	275	–0.27	04/93
09 02	5.61	28 00	18.1	0.86*	4.53	18.66	1.22	1.31	168	–0.26	04/93
09 58	17.68	29 26	4.3		0.76	18.22	0.89	0.47	162	> 0.38	04/92
10 59	39.86	59 57	28.5	1.83	1.24	16.73	0.76	0.17	250	–0.21	04/93
11 00	29.73	30 30	52.3	0.38	1.76	17.50	0.53	0.46	211	–0.14	04/93
11 24	13.75	45 32	36.6	1.81	0.23	16.98	0.41	0.46	355	–0.26	04/93
11 28	3.36	30 48	8.0	0.74	0.99	17.73	0.70	0.76	377	–0.16	04/93
11 45	24.06	26 52	22.0	0.87	0.63	17.40	0.54	0.71	381	–0.07	04/93
12 02	4.32	52 45	23.5	2.73	0.32	17.88	0.67	0.14	228	–0.52	04/93
12 06	51.10	41 36	22.4		0.48	16.35	0.86	0.48	515	0.37	04/93
12 18	59.03	44 28	7.6	1.35	1.28	17.35	0.73	0.27	478	–0.18	04/93
15 50	49.07	78 54	23.2		3.03	19.02	> 2.96	2.76	166	–0.77	04/93
15 57	41.39	56 33	41.4		0.40	16.65	0.99	0.91	215	–0.38	04/92
17 53	56.18	64 52	29.0		3.60	18.30	1.52	0.27	267	0.61	04/92
22 09	45.67	23 40	49.2		0.61	18.89	0.70	0.62	1212	0.69	10/92
22 26	12.04	27 51	40.1	0.59*	1.65	18.70	0.14	0.41	160	–0.53	10/92
23 21	14.36	27 18	50.8	1.69*	0.53	18.95	0.96	1.35	186	–0.38	10/92

**Table 5.** Objects from the complete sample with no spectra or very poor spectra.

$\alpha$	Optical Position			$N\sigma_c$	E mag	O–E mag	$\Delta r$ "	$S_5$ mJy	$\alpha_{1.4}^5$	Comments	
	1950	$\delta$									
00	55	47.54	32 55	7.1	0.53	19.87	1.13	1.10	164	-0.15	WHT 10/92 No object detected
03	58	49.05	21 02	8.3	0.09	17.94	1.23	0.43	158	-0.68	No spectrum taken
13	21	58.84	41 03	48.9	0.16	19.49	2.56	0.57	413	0.11	WHT 04/92 low s/n
16	56	24.93	48 13	3.8	0.04	19.55	> 2.37	0.83	847	-0.12	WHT 04/93 No object detected

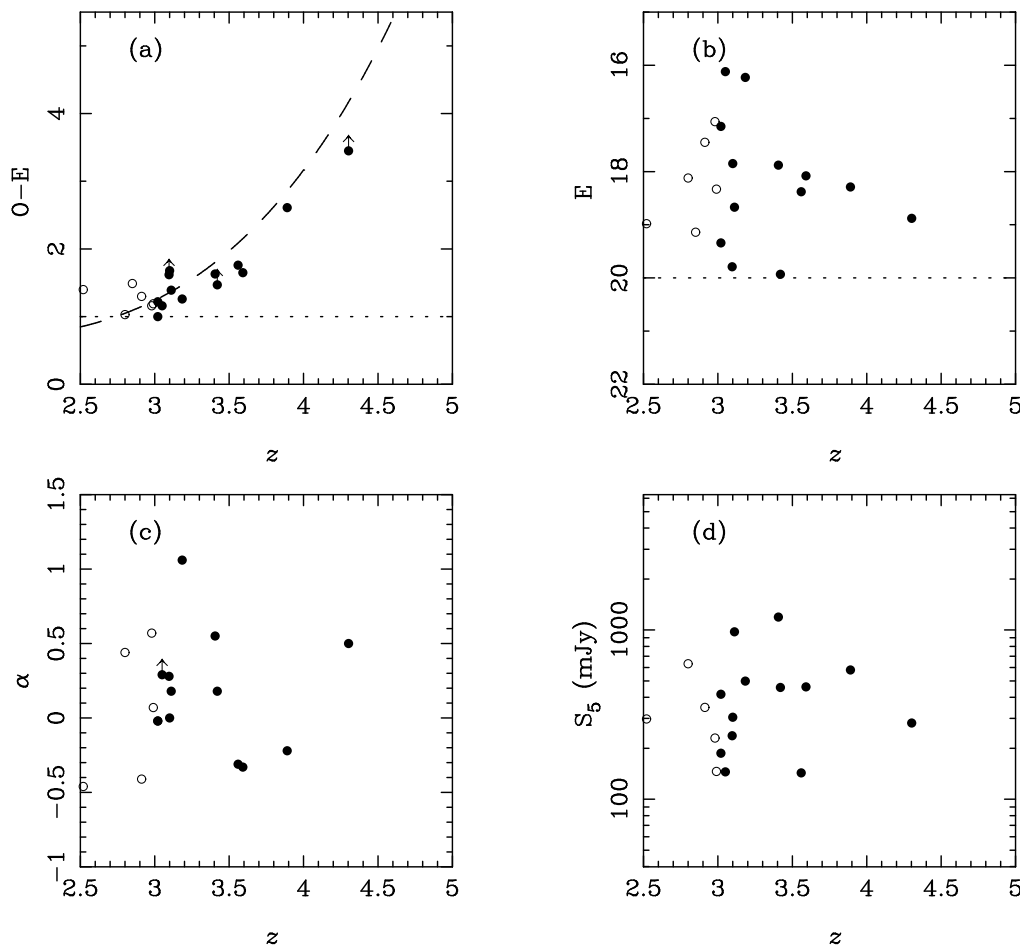


**Figure 7.** (a)  $O - E$  colour versus  $z$ , (b)  $E$  magnitude versus  $z$ , (c) spectral index  $\alpha$  versus  $z$ , (d) 5-GHz Radio flux  $S_5$  versus  $z$  for objects with  $z > 2.5$  in the complete sample. The horizontal dotted lines in (a) and (b) show the limits imposed on the parameters in constructing the sample. The dashed curve in (a) shows a fit obtained using  $O - E$  versus  $z$  data for a sample of optically selected quasars. Objects that did not appear on the O plate are shown with arrows in (a). Objects with  $2.5 < z < 3.0$  are shown with open circles – the survey is substantially incomplete for these objects.

*GB1623+5748* Vermeulen et al. (1996) obtain a redshift  $z = 0.789 \pm 0.001$  for this source based on the [OIII] doublet, not visible in our spectrum.

*GB1745+6227* This object has been independently discovered by Becker, Helfand & White (1992) on the basis of its X-ray emission. They report a redshift of 3.87, which is lower than the value derived here. Stickel & Kühr (1993a) report a redshift of 3.886, in close agreement with the value derived in this work.

*GB1747+4322* Vermeulen et al. (1996) also find this to be featureless after 3000s on the Hale telescope.

*GB1759+7539* This object, with  $z = 3.05$ , is optically very bright ( $E=16.1$  mag).

*GB2319+4429* Henstock (in preparation) also finds this to be featureless after 3000s on the INT.

*GB2342+3417* White, Kinney & Becker (1993) report  $z = 3.01$  compared with our measurement of  $z = 2.99$ .

Finding charts and spectra for *GB1508+5714* and *GB1745+6227* have already been given by Hook et al. (1995), and are included here for completeness (Figures 6 and 8).

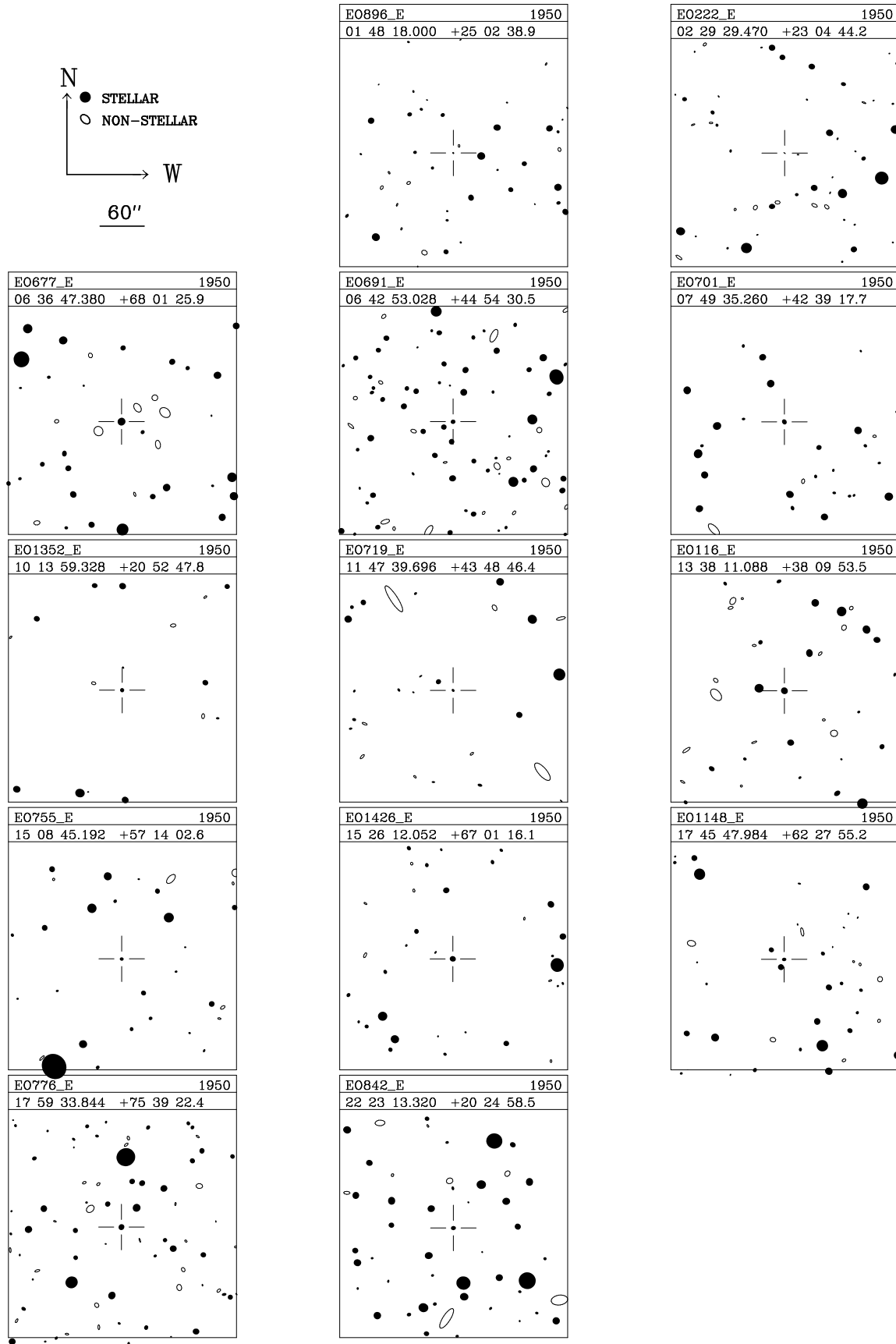


**Figure 8.** Finding charts from APM scans of POSS-I E plates ( $\sim R$  band) for the  $z > 3$  QSOs in the complete sample.

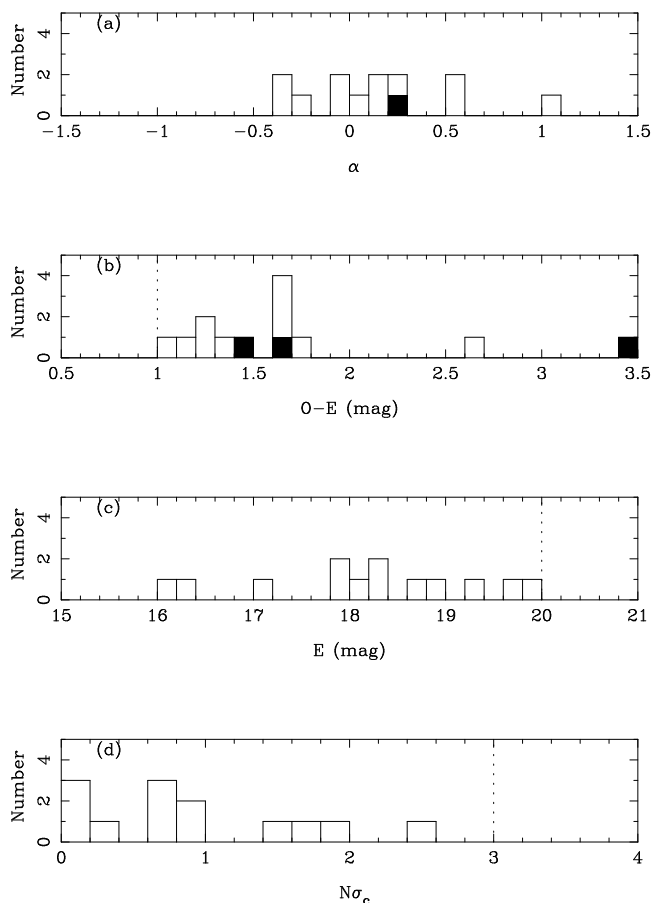


**Figure 6.** The distributions of the 13  $z > 3$  quasars of the complete sample in terms of (a) spectral index  $\alpha$ , (b) colour  $O-E$ , (c) apparent  $E$  magnitude and (d) classification parameter  $N\sigma_c$ . The filled histogram in (b) indicates the contribution in each bin from objects that did not appear on the  $O$  plate, hence these  $O-E$  values are lower limits. Similarly in (a) the filled histogram shows the object with a lower limit on  $\alpha$ . The vertical dotted lines show the limits imposed on the parameters in constructing the sample.

## 7 CONCLUSIONS

In conclusion, we have shown that the radio/colour selection method is a highly successful technique for finding  $z > 3$  QSOs. This paper provides the first large, well-defined sample of radio-loud QSOs with  $z > 3$ .

We are obtaining follow-up observations of two other radio samples, the 100-mJy ‘MG-VLA’ sample (Lawrence et al. 1986) and a 50-mJy sample (Lehár 1991). These samples combined with that used in this paper contain a total of  $\sim 6000$  radio sources, and the total area optically identified using the APM covers  $3.7\text{sr}$  ( $12\,000\text{ deg}^2$ ) of sky.

## ACKNOWLEDGMENTS

We are very grateful to Alok Patnaik, Ian Browne, Peter Wilkinson and Joan Wrobel for supplying the radio catalogue used in this work prior to publication. We thank Lisa Storrie-Lombardi for help in obtaining the spectra and reducing the data for GB1745+6227. We also thank Rene Vermeulen for checking our redshifts against those in the

CJ1/CJ2 data base. IMH acknowledges a NATO postdoctoral fellowship and RGM thanks the Royal Society for support. This research has made use of the NASA/IPAC Extragalactic Database (NED) which is operated by the Jet Propulsion Laboratory, Caltech, under contract with the National Aeronautics and Space Administration. IRAF is distributed by the National Optical Astronomy Observatories, which is operated by the Association of Universities for Research in Astronomy, Inc. (AURA) under cooperative agreement with the National Science Foundation.

## REFERENCES

- Aller M. F., Aller H. D., Hughes P. A., 1992, *ApJ*, 399, 16  
 Allington-Smith J. R. et al 1989, *MNRAS*, 238, 603  
 Bade N., Fink H. H., Engels D., Voges W., Hagen H.-J., Wisotzki L., Reimers D., 1995, *A&AS*, 110, 469  
 Becker R. H., White R. L., Edwards A. L., 1991, *ApJS*, 75, 1  
 Becker R. H., Helfand D. J., White R. L., 1992, *ApJ*, 104, 531  
 Bunclark P. S., Irwin M. J., 1983, in Rolfe E. J., ed., *Proc. Statistical Methods in Astronomy*, ESA SP-201. ESA, Noordwijk, p.195  
 Carswell R. F., Strittmatter P. A., 1973, *Nat*, 242, 394  
 Condon J. J., Broderick J. J., 1985, *AJ*, 90, 2540  
 Condon J. J., Broderick J. J., 1986, *AJ*, 91, 1051  
 Condon J. J., Broderick J. J., Seielstad G. A., 1989, *AJ*, 97, 1064  
 Crampton D., 1991, ed., *The Space Distribution of Quasars*. Astron. Soc. Pac., San Francisco, vol.21  
 Dunlop J. S., Peacock J. A., 1990, *MNRAS*, 247, 19  
 Fleming T. A., Green R. F., Jannuzi B. T., Liebert J., Smith P. S., Fink H., 1993, *AJ*, 106, 1729  
 Gearhart M. J., Lund J. M., Frantz D. J., Kraus J. D., 1972, *AJ*, 77, 557  
 Gregory P. C., Condon J. J., 1991, *ApJ*, 75, 1011  
 Hartwick F. D. A., Schade D., 1990, *ARA&A*, 28, 437  
 Hazard C., 1986, in Wall J. V., Boksenberg A. eds, *Proc. Modern Instrumentation and its Influence on Astronomy*. Cambridge Univ. Press, Cambridge, p157  
 Hazard C., Mackey C. B., Shimmins A. J., 1963, *Nat*, 197, 1037  
 Hazard C., McMahon R. G., Sargent W. L. W., 1986, *Nat*, 322, 38  
 Hewitt A., Burbidge G., 1987, *APJS*, 63, 1  
 Hewitt A., Burbidge G., 1989, *APJS*, 69, 1  
 Hook I. M., McMahon R. G., Patnaik A. R., Browne I. W. A., Wilkinson P. N., Irwin M. J., Hazard C., 1995, *MNRAS*, 273, L63  
 Irwin M., McMahon R. G., Hazard C., 1991, in Crampton D., ed., *ASP Conf. Ser. Vol 21, The Space Distribution of Quasars*. Astron. Soc. Pac., San Francisco, p. 117  
 Kühr H., 1977, *A&AS*, 29, 139  
 Kühr H., 1980, PhD thesis, Univ. Bonn  
 Kühr H., Pauliny-Toth I. I. K., Witzel A., Schmidt J., 1981, *AJ*, 86, 854  
 Kulkarni V. K., Mantovani F. Pauliny-Toth I. I. K. 1990, *A&AS*, 82, 41  
 Lawrence C. R., Bennett C. L., Hewitt J. N., Langston G. I., Klotz S. E., Burke B. F., 1986, *ApJS*, 61, 105  
 Lehár J., 1991, PhD thesis, Massachusetts Institute of Technology  
 McMahon R. G., 1991, in Crampton D., ed., *ASP Conf. Ser. Vol. 21, The Space Distribution of Quasars*. Astron. Soc. Pac., San Francisco, p.129  
 Meisenheimer K., Röser H.-J., 1983, *A&AS*, 51, 41  
 Miller L. P., Mitchell P. S., Boyle B. J., 1990, *MNRAS*, 244, 1  
 Osmer P. S., Porter A. C., Green R. F., Foltz C. B., 1988, eds, *ASP Conf. Ser. vol. 2, Proc. Workshop on Optical Surveys for Quasars*. Astron. Soc. Pac., San Francisco

- Owen F., Ledlow M. J., Keel W. C., 1995, *AJ*, 109, 14
- Patnaik A., Narasimha D., 1993, *Bull. Astron. Soc. India*, 21, 457
- Patnaik A. R., Browne I. W. A., Wilkinson P. N., Wrobel J. M., 1992a, *MNRAS*, 254, 655
- Patnaik A. R., Browne I. W. A., Walsh D., Chaffee F. H., Foltz C. B., 1992b, *MNRAS*, 259, 1
- Patnaik A. R., Browne I. W. A., King L. J., Muxlow T. W. B., Walsh D., Wilkinson P. N., 1993, *MNRAS*, 261, 435
- Peacock J. A., 1985, *MNRAS*, 217, 610
- Polatidis A.G., Wilkinson P.N., Xu W., Readhead A.C.S., Pearson T. J., Taylor G. B., Vermeulen R. C., 1995, *ApJS*, 98, 1
- Schmidt M., 1963, *Nat*, 197, 1040
- Schmidt M., 1968, *ApJ*, 151, 393
- Schmidt M., Schneider D. P., Gunn J. E., 1991 in Crampton D., ed., *ASP Conf. Ser. Vol. 21, The Space Distribution of Quasars. Astron. Soc. Pac., San Francisco*, p.109
- Schneider D. P., Schmidt M., Gunn J., 1994, *AJ*, 107, 1245
- Stickel M., Kühr H., 1993a, *A&AS*, 100, 395
- Stickel M., Kühr H., 1993b, *A&AS*, 101, 521
- Stickel M., Kühr H., 1994, *A&AS*, 103, 349
- Taylor G.B., Vermeulen R.C., Pearson T.J., Readhead A.C.S., Henstock D. R., Browne I. W. A., Wilkinson P. N., 1994, *ApJS*, 95, 345
- Vermeulen R. C., Taylor G. B., 1995, *AJ*, 109, 1983
- Vermeulen R.C., Taylor G.B. Readhead A.C.S. Browne I.W.A., 1996, *AJ*, 111, 1013
- Véron-Cetty M. P., Véron P., 1991, *ESO Sci. Rep.*, No. 10
- Warren S. J., Hewett P. C., Osmer P. S., 1991, *ApJS*, 76, 23
- Warren S. J., Hewett P. C., Osmer P. S., 1994, *ApJ*, 421, 412
- White R. L., Becker R. H., 1992, *ApJS*, 79, 331
- White R. L., Kinney A. L., Becker R. H., 1993, *ApJ*, 407, 456
- Xu W., Lawrence C. R., Readhead A. C. S., Pearson T. J., 1994, *AJ*, 108, 395